

Very High Energy Afterglow Emission of GRB 221009A: Lessons Learned from the Brightest Long Gamma-ray Burst in a Wind Environment

JIA REN,^{1,2} YUN WANG,^{3,4} AND LU-LU ZHANG⁵

¹*School of Astronomy and Space Science, Nanjing University, Nanjing 210023, China*

²*Key Laboratory of Modern Astronomy and Astrophysics (Nanjing University), Ministry of Education, Nanjing 210023, China*

³*Key Laboratory of Dark Matter and Space Astronomy, Purple Mountain Observatory, Chinese Academy of Sciences, Nanjing 210034, China*

⁴*Department of Astronomy, School of Physical Sciences, University of Science and Technology of China, Hefei 230026, China*

⁵*Guangxi Key Laboratory for Relativistic Astrophysics, School of Physical Science and Technology, Guangxi University, Nanning 530004, China*

Submitted to ApJL

ABSTRACT

In this paper, we modeled the dynamics and radiation physics of the rarity event GRB 221009A afterglow in detail. Based on the analysis results of the ASGAR package we developed, the afterglow data of GRB 221009A strongly favors the origin of a relativistic jet propagating in a stellar-wind-dominated environment. Therefore, GRB 221009A is a typical lesson for the very high energy (VHE) afterglow of long gamma-ray burst in a wind environment. We also show the broadband spectral energy distribution (SED) analysis results of GRB 221009A, and find that the synchrotron self-Compton (SSC) radiation component of GRB 221009A is very bright in the 0.1 – 10 TeV band. The integrated SED of 0 – 2000 s after *Fermi*/GBM trigger shows that the bright SSC component can be easily observed in TeV band, above the detection sensitivity of LHAASO, MAGIC and CTA. We predict that the SSC radiation peak flux of GRB 221009A in the first 2000 second integral SED is $\sim 10^{-7}$ erg cm⁻² s⁻¹, with a peak energy close to 300 GeV. Furthermore, we find that the inclusion of GeV observations could break the degeneracy between model parameters, highlighting the significance of high-energy observations in determining accurate parameters for GRB afterglows.

Keywords: Gamma-ray bursts (629); High energy astrophysics (739)

1. INTRODUCTION

On 2022 October 9 at 13:16:59.000 UT, the *Fermi* Gamma-Ray Burst Monitor (GBM) triggered long duration gamma-ray burst GRB 221009A (Veres et al. 2022). Not too late, at 14:10:17 UT, The *Swift* Burst Alert Telescope (BAT) triggered GRB 221009A, aka Swift J1913.1+1946 (Dichiara et al. 2022). The *Fermi* Large Area Telescope (LAT) detected high-energy

emission from GRB 221009A at 14:17:05.99 (Bissaldi et al. 2022a), and the high energy photon observed by *Fermi*/LAT reaches 99.3 GeV (Pillera et al. 2022), even 397.7 GeV (Xia et al. 2022). The *Swift* X-ray Telescope (XRT) have fruitful follow up observations (Bissaldi et al. 2022b). GRB 221009A is extraordinary bright with isotropic prompt emission energy $E_{\gamma, \text{iso}} = 2 - 3 \times 10^{54}$ erg by assuming the redshift $z = 0.1505$ (de Ugarte Postigo et al. 2022b; Castro-Tirado et al. 2022). Very energetic GRBs at such close distances are estimated to occur only once in decades or even a century (Atteia 2022), and it is possible to detect very high energy (VHE) photons (Xue et al. 2009). As expected, China's Large High Altitude Air Shower Observatory (LHAASO) recorded tens of thousands of photon signals in the VHE region above 100 GeV, including photons with energy greater than 10 TeV (Huang et al. 2022),

Corresponding author: Jia Ren
jia@smail.nju.edu.cn

Corresponding author: Yun Wang
wangyun@pmo.ac.cn

Corresponding author: Lu-Lu Zhang
deer@st.gxu.edu.cn

which can give the finest measurement of the lightcurve in the highest energy band of GRBs.

In recent years, several long GRBs have been successfully observed corresponding VHE afterglows. Long GRBs with the same VHE afterglows as GRB 221009A, including GRBs 180720B, 190114C, 190829A, 201015A, and 201216C, have four orders of magnitude on $E_{\gamma, \text{iso}}$ from $\sim 10^{50}$ erg to $\sim 10^{54}$ erg. The VHE afterglow of GRB 180720B ($E_{\gamma, \text{iso}} = 6 \times 10^{53}$ erg at $z = 0.654$) were firstly detected with the High Energy Stereoscopic System (H.E.S.S.) in a confidence level of 5.3σ in the 0.1 – 0.4 TeV band (Abdalla et al. 2019). Moreover, the VHE afterglow of GRB 190114C ($E_{\gamma, \text{iso}} = 3 \times 10^{53}$ erg at $z = 0.4245$) was convincingly detected with the Major Atmospheric Gamma Imaging Cerenkov (MAGIC) telescopes in the 0.3 – 1 TeV band in a high confidence level of $> 50\sigma$ (MAGIC Collaboration et al. 2019). The TeV afterglow of nearby GRB 190829A was detected ($E_{\gamma, \text{iso}} = 2 \times 10^{50}$ erg at $z = 0.0785$) with H.E.S.S. in the 0.2 – 4 TeV band with a confidence level of 21.7σ (H. E. S. S. Collaboration et al. 2021). The VHE afterglows of GRBs 201015A (> 140 GeV, 3.5σ , Suda et al. 2021) and 201216C (~ 100 GeV, 6σ , Fukami et al. 2021) were detected by the MAGIC telescopes also, but the data have not yet been released. These two bursts have prompt emission energy $E_{\gamma, \text{iso}} = 1.1 \times 10^{50}$ erg with the redshift $z = 0.423$ of GRB 201015A, and $E_{\gamma, \text{iso}} = 5.76 \times 10^{53}$ erg with the redshift $z = 1.1$ of GRB 201216C, respectively (Zhang et al. 2022, in preparation). Since the extragalactic background light (EBL) absorbs sub-TeV/TeV photons from high-redshift sources, the VHE afterglows of low-redshift GRBs should be easier to detect (e.g., Finke et al. 2010; Domínguez et al. 2011). Overall, it seems that both energetic and sub-energetic GRBs can accelerate the particles to an extremely high energy and produce the VHE afterglows (e.g. Hurley et al. 1994; Murase et al. 2006).

The new window opened on TeV emission of GRBs usher in a new era of GRB physics at extremely high energies. The VHE afterglows of GRBs are generally believed to be attributed to synchrotron, synchrotron self-Compton (SSC), and/or external inverse-Compton (EIC) radiations of the electrons accelerated in relativistic jets (e.g., Dermer et al. 2000; Zhang & Mészáros 2001; Sari & Esin 2001; He et al. 2009; MAGIC Collaboration et al. 2019; Acciari et al. 2021; H. E. S. S. Collaboration et al. 2021; Zhang et al. 2021; Zhang et al. 2021). To distinguishing between these components, accurate modeling of broadband spectral energy distributions (SEDs) is required. Thus, abundant and high-quality observations from radio to TeV at same timescales for SEDs and continuously monitored multiband

afterglow lightcurves will provide a powerful support for understanding the physics of GRB radiation (e.g., Wang et al. 2019; Zhang et al. 2020; Joshi & Razzaque 2021; Yamasaki & Piran 2022).

It is widely accepted that long GRBs can occur during the collapse of stars. Accordingly, stars may have undergone a drastic material-loss process before finally collapsing, resulting in circumburst environments dominated by stellar winds. Previous works have inferred that GRB 190114C maybe occur in stellar wind environment, but other possibilities have not been ruled out (e.g., Asano et al. 2020; Joshi & Razzaque 2021). In this Letter, we find that the afterglow lightcurve and SED of GRB 221009A strongly support this occurrence. It makes GRB 221009A the first long GRB with clear indications of occurring in a wind environment to produce VHE afterglow.

This paper is organized as follows. In Section 2, we briefly describe the analysis and collection of observational data. In Section 3, we introduce our model considerations in detail and present the results of model parameter inference. We summarize and discuss the significance of our results in Section 4. We take the cosmology parameters as $H_0 = 67.8 \text{ km s}^{-1} \text{ Mpc}^{-1}$, and $\Omega_M = 0.308$ (Planck Collaboration et al. 2016).

2. MULTIWAVELENGTH OBSERVATION AND SPECTRAL ANALYSIS OF GRB 221009A

2.1. *Fermi*/LAT data analysis

Fermi/LAT is a pair conversion telescope covering a wide energy band (from 20 MeV to greater than 300 GeV, Atwood et al. 2009). We analyze the observation data of *Fermi*/LAT in the direction of GRB 221009A (RA = 288.282, Dec = 19.495, from Pillera et al. (2022) based on the standard procedure¹. Considering the duration and high-energy events of GRB 221009A (Xia et al. 2022), data were extracted with the energy range of 100 MeV to 1 TeV, using transient event class (ev-class=16) before 400 seconds and source event class (ev-class=128) after that, and the corresponding instrument response functions (IRFs) file are used in the unbinned likelihood analysis. In addition to using `pyLikelihood` to call some functions of `Fermitools`, we also use some user-contributed tools², for example, `make4FGLxml` is used to generate xml model files, `gtapps_mp` is used to multithread some commands, and `likeSED` is used for spectral energy distribution analysis of unbinned likelihood. Considering possible pile-up effects (Omodei et al.

¹ <https://fermi.gsfc.nasa.gov/ssc/data/analysis/scitools/>

² <https://fermi.gsfc.nasa.gov/ssc/data/analysis/user/>

2022), we did not use LAT data in the time intervals $T_0 + 225$ to $T_0 + 236$ seconds and $T_0 + 257$ to $T_0 + 265$ seconds, where T_0 is the trigger time of *Fermi*/GBM (Veres et al. 2022).

2.2. Other follow-up observations observations

We collected follow-up observations that have been reported from GCN³ or ATel⁴. For the *Swift*/XRT observation data, we rebin the 0.3-10 keV light curve based on the counts per bin (PC=600, WT=200)⁵, from about 3300 seconds to 2.3 days after *Fermi*/GBM trigger. We take into account the information of the time-resolved spectrum into the converting count-rates to energy fluxes from the spectral evolution data given by the “burst analyzer” tool⁶ (see more details in Evans et al. 2007, 2009). And, the *Swift*/XRT spectrum in the different time slices we used were extracted by an online analysis tool⁷. We have collected the optical data (r , r' , R and z -band, Hu et al. 2022; Belkin et al. 2022b; de Wet & Groot 2022; Brivio et al. 2022; Gregory et al. 2022; Kumar et al. 2022; Chen et al. 2022; Zheng et al. 2022; Kim et al. 2022; Groot et al. 2022; Belkin et al. 2022a; Watson et al. 2022; Strausbaugh & Cucchiara 2022; Vinko et al. 2022; Zaznobin et al. 2022; Bikmaev et al. 2022a,b; Huber et al. 2022; Shrestha et al. 2022a,b; Brethauer et al. 2022) and radio data (frequencies around 1.5 GHz, 5 GHz, 15 GHz and 90 GHz, Bright et al. 2022; Farah et al. 2022; de Ugarte Postigo et al. 2022a; Rhodes et al. 2022; Laskar et al. 2022; Urata et al. 2022; Trushkin et al. 2022) for our model analysis. In addition, the High-Altitude Water Cherenkov Observatory (HAWC) has reported their observation result started from ~ 8 hours after the trigger time and lasted ~ 3.4 hours. Assuming a power law spectrum with photon index of -2.0, they found no significant detection and proceeded to calculate the 95% upper limit on the flux at 1 TeV as 4.16×10^{-12} TeV cm² s⁻¹ (HAWC collaboration 2022).

2.3. Joint spectral analysis of X-ray and optical band

We have exam the optical band whether exist to the host galaxy extinction or not. The joint spectral analysis of X-ray and optical afterglows at the timeslice from 5.3×10^4 to 5.7×10^4 seconds is using XSPEC (version 12.12.1) package. The above epoch including R , I , B , V band and they are AB magnitude except for

³ <https://gcn.gsfc.nasa.gov>

⁴ <https://www.astronomerstelegram.org>

⁵ https://www.swift.ac.uk/xrt_curves/

⁶ https://www.swift.ac.uk/burst_analyser/

⁷ https://www.swift.ac.uk/xrt_spectrum/

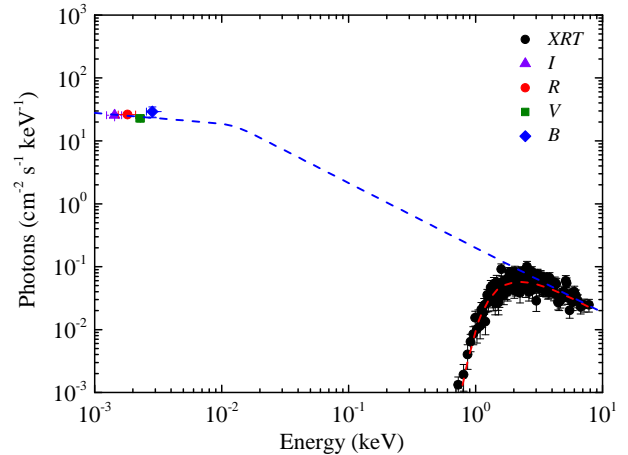


Figure 1. Joint optical-X-ray afterglow observed in the time interval of $[5.3 \sim 5.7] \times 10^4$ seconds of GRB 221009A along with our fit with a broken power-law function (the red dashed line). The optical data are extinction-corrected for our Galaxy. The H I absorption of our Galaxy is also considered in our spectral fit. The blue dashed line is plotted by using the model parameters of photon indices and break energy.

the B band (Gregory et al. 2022; Zheng et al. 2022). The Galactic extinction of four band are $A_R = 4.262$, $A_I = 3.093$, $A_V = 5.286$ and $A_B = 6.881$, respectively (Schlegel et al. 1998). We notice that the Galactic extinction is very strong, which is corresponding to the reddening of $E_{B-V} = 1.563$ in the direction of the burst (Kuin & Dichiara 2022). The Galactic H I column density $N_{\text{H}}^{\text{Gal}} = 5.36 \times 10^{21}$ cm⁻² at the GRB direction is fixed. The extinction curve of the host galaxy is taken as the same of Mike Way (MW) (Pei 1992) by setting $R_V = 3.08$. We find that the extinction value of the host galaxy with the absorption model is very small and negligible. Finally, we fit the joint spectrum of X-ray-optical afterglow with a broken power-law model and the derived photon index are $\Gamma_{\text{O,X}}^1 = 1.17 \pm 0.19$ and $\Gamma_{\text{O,X}}^2 = 2.03 \pm 0.08$. The break energy is $E_{\text{break}} = (1.25 \pm 0.97) \times 10^{-2}$ keV. The reduced χ^2 is $142.23/143 = 1.0$. The fitting result is shown in Figure 1. Hence, the extinction in the optical band of the host galaxy is negligible, which suggests a heavy extinction from the Galactic and the host galaxy have no impact for optical radiation of GRB 221009A.

3. PHYSICAL IMPLICATION

3.1. Afterglow model Inference

We try to explain the multiband observations of GRB 221009A from radio to GeV band and infer the physical parameters through the afterglow model. The afterglow model is based on a Python-Fortran hybrid code ASGAR package we developed and can be modi-

fied for different physical considerations (e.g., [Ren et al. 2020](#)). In this work, we consider the synchrotron radiation and SSC processes of electrons in the jet to generate realistic radiation behavior. We will briefly describe the

main numerical methods and model used in the following.

The dynamics of the external-forward shock of the jet described as ([Nava et al. 2013](#); [Zhang 2018](#)),

$$\frac{d\Gamma}{dr} = -\frac{\Gamma(\Gamma^2 - 1)(\hat{\gamma}\Gamma - \hat{\gamma} + 1)\frac{dm}{dr}c^2 - (\hat{\gamma} - 1)\Gamma(\hat{\gamma}\Gamma^2 - \hat{\gamma} + 1)(3U/r)}{\Gamma^2[m_0 + m]c^2 + (\hat{\gamma}^2\Gamma^2 - \hat{\gamma}^2 + 3\hat{\gamma} - 2)U}, \quad (1)$$

$$\frac{dU}{dr} = (1 - \epsilon)(\Gamma - 1)c^2\frac{dm}{dr} - (\hat{\gamma} - 1)\left(\frac{3}{r} - \frac{1}{\Gamma}\frac{d\Gamma}{dr}\right)U, \quad (2)$$

where $dm/dr = n(r)m_p r^2$ with $n(r)$ being the particle density of circum-burst medium and m_p being the proton mass, and $\Gamma(r)$, $m(r)$, $U(r)$, and ϵ are the bulk Lorentz factor, the swept-up mass, the internal energy, and the radiation efficiency of electrons in the external-forward shock, respectively. The adiabatic index is $\hat{\gamma} \simeq (5 - 1.21937\zeta + 0.18203\zeta^2 - 0.96583\zeta^3 + 2.32513\zeta^4 - 2.39332\zeta^5 + 1.07136\zeta^6)/3$ with $\zeta \equiv \Theta/(0.24 + \Theta)$, $\Theta \simeq (\Gamma\beta/3)[\Gamma\beta + 1.07(\Gamma\beta)^2]/[1 + \Gamma\beta + 1.07(\Gamma\beta)^2]$, and $\beta = \sqrt{1 - 1/\Gamma^2}$ ([Pe'er 2012](#)). We have numerically solved equations (1) and (2) with the forth-order Runge-Kutta method. ϵ_e and ϵ_B are the equipartition factors for the energy in electrons and magnetic field in the shock, respectively. Then, the magnetic field behind the shock is $B' = [32\pi\epsilon_B n(r)]^{1/2}\Gamma c$, where “ r ” marks the co-moving frame of shock. The swept-in electrons by the shock are accelerated to a power-law distribution of Lorentz factor γ_e , i.e., $Q \propto \gamma_e^{-p}$ for $\gamma'_{e,\min} \leq \gamma_e \leq \gamma'_{e,\max}$, where $p(> 2)$ is the power-law index, $\gamma_{e,\min} = \epsilon_e(p-2)m_p\Gamma/[(p-1)m_e]$ ([Sari et al. 1998](#)), and $\gamma_{e,\max} = \sqrt{9m_e^2c^4/[8B'q_e^3(1+Y)]}$ with q_e being the electron charge ([Kumar et al. 2012](#)), where Y is the Compton parameter. Then, one can have $\epsilon = \epsilon_{\text{rad}}\epsilon_e$ with $\epsilon_{\text{rad}} = \min\{1, (\gamma_{e,\min}/\gamma_{e,c})^{(p-2)}\}$ ([Sari & Esin 2001](#); [Fan et al. 2008](#)), where $\gamma_{e,c} = 6\pi m_e c/[\sigma_T\Gamma B'^2 t'(1+Y)]$ is the efficient cooling Lorentz factor of electrons with σ_T being the Thomson scattering cross section.

We denote the instantaneous electron spectrum as $dN_e/d\gamma'_e$, of which the evolution can be solved based on the continuity equation of electrons,

$$\frac{\partial}{\partial t'}\left(\frac{dN_e}{d\gamma'_e}\right) + \frac{\partial}{\partial \gamma'_e}\left[\dot{\gamma}'_{e,\text{tot}}\left(\frac{dN_e}{d\gamma'_e}\right)\right] = Q(\gamma'_e, t'), \quad (3)$$

We refer to [Fan et al. \(2008\)](#) for the way to solve this equation. We note the Compton parameter $Y(\gamma'_e)$ has solved basing on the work of [Fan & Piran \(2006\)](#). On the numerical method, we solve the continuity equation using a finite difference method of the third-order total-variation-diminishing Runge-Kutta method of time t'

(TVD+RK3) and fifth-order weighted essentially non-oscillatory method of γ'_e (WENO5, [Jiang & Shu 1996](#)).

In the X-ray/optical/radio bands, the main radiation mechanism of the electrons in GRB jets is synchrotron radiation ([Sari et al. 1998](#); [Sari & Piran 1999](#)). The spectral power of synchrotron radiation of $n'_e(r, \gamma'_e)$ at a given frequency ν' is

$$P'(\nu', r) = \frac{\sqrt{3}q_e^3 B'}{m_e c^2} \int_0^{\gamma'_{e,\max}} F\left(\frac{\nu'}{\nu'_c}\right) n'_e(r, \gamma'_e) d\gamma'_e, \quad (4)$$

where $F(x) = x \int_x^{+\infty} K_{5/3}(k) dk$ with $K_{5/3}(k)$ being the modified Bessel function of 5/3 order and $\nu'_c = 3q_e B' \gamma_e'^2 / (4\pi m_e c)$.

The emission of the SSC process is calculated based on the electron spectrum and seed photons from the synchrotron radiation (e.g., [Geng et al. 2018](#); [Huang 2022](#)). We have numerically solved the Klein-Nishina effect and the $\gamma\gamma$ annihilation effects (e.g., [Gould & Schröder 1967](#); [Fan et al. 2008](#); [Nakar et al. 2009](#); [Murase et al. 2011](#); [Geng et al. 2018](#)).

We set the GRB jet as an on-axis-observed top-hat jet without considering the lateral expansion. The effect of the equal-arrival-time surface (EATS) is considered (e.g., [Waxman 1997](#)). We divide the radiation surface as small rings for the on-axis-observed jet. The intrinsic SEDs can be obtained from the integration over the EATS after considering the Doppler boosting effect. The EBL absorption effect is taken into account for calculating the observed high energy photons ([Domínguez et al. 2011](#)). By summing the flux from each ring observed at a same observer time, the total observed flux can be obtained.

3.2. Inference Results

We use the `emcee` Python package ([Foreman-Mackey et al. 2013](#)) to fit the light curves from radio to GeV energy bands and perform parameters inference, including the isotropic kinetic energy $E_{k,\text{iso}}$, ϵ_e , ϵ_B , p , the initial bulk Lorentz factor Γ_0 , the half-opening angle of jet θ_j , and the wind parameter A_\star . Note that the number density of medium $n(r) = 3 \times 10^{35} A_\star r^{-2} \text{ cm}^{-3}$. Besides, we have aligned the observation times of the

Table 1. Multiband Fitting Results with the Forward Shock Model

GRB	$\log_{10} E_{k, \text{iso}}$ (erg)	$\log_{10} \Gamma_0$	p	$\log_{10} \epsilon_e$	$\log_{10} \epsilon_B$	$\log_{10} \theta_j$	$\log_{10} A_*$
221009A	$54.83^{+0.10}_{-0.08}$	$2.28^{+0.02}_{-0.03}$	$2.60^{+0.03}_{-0.02}$	-0.69 ± 0.02	$-2.73^{+0.07}_{-0.10}$	$-1.61^{+0.06}_{-0.06}$	$-1.91^{+0.01}_{-0.01}$

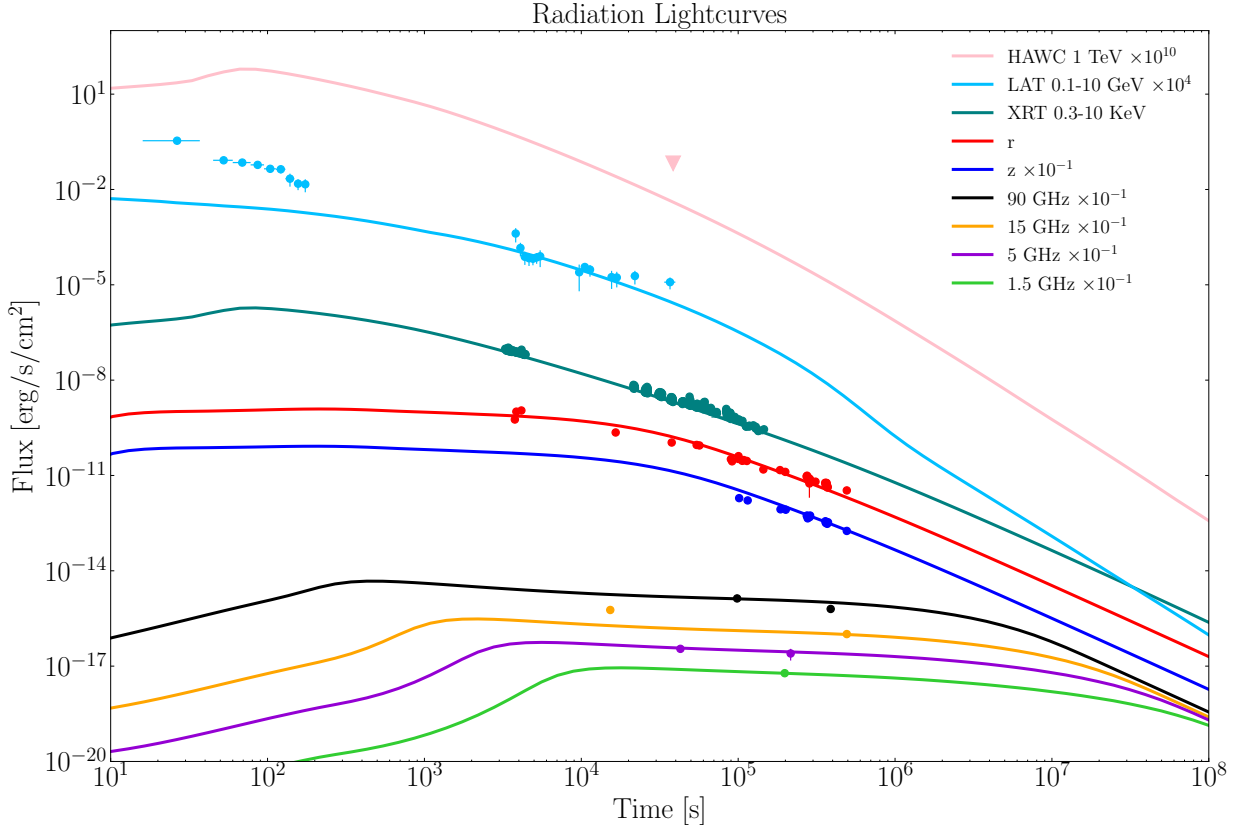


Figure 2. Multiband lightcurves from radio to TeV band plotted with our best fitting result. The jet generation time is set at $T_0 + 220$ s with T_0 being the trigger time of *Fermi*/GBM. The optical data have performed the Galactic extinction correction, and the light curve at 1 TeV has considered the EBL absorption. We show the HAWC 1 TeV upper limit at $T_0 + 8$ hours.

Swift/XRT data with the trigger time T_0 reported by the *Fermi*/GBM. Considering that the precursor radiation is observed when the GBM trigger, the energy of precursor is not sufficient to drive a powerful jet. Hence we set the generation time of an energetic jet as $\sim T_0 + 220$ s, which is the time of the main burst start. Furthermore, we also have considered the Galactic extinction in the r and z bands which are $A_r = 4.31$ mag and $A_z = 2.317$ mag, respectively⁸. And the extinction from host galaxy seems insignificant as mentioned above, so it has been ignored in our analysis.

We have examined the possibility of GRB 221009A that took place in a typical interstellar medium (ISM)

environment. We find that for reasonable parameters the model curves are always higher than the observed data reported in radio bands, say, the radio observations strongly reject the ISM environment. As a result, we find that the multiband afterglow of GRB 221009A can be explained by a relativistic jet propagate in the circumburst environment dominated by a stellar wind. Our fitting results are shown in Figure 2. The derived model parameters are reported in Table 1, and their posterior distributions are shown in Figures 3.

It shows that the initial $\sim T_0 + 400$ s GeV emission observed by *Fermi*/LAT in Figure 2 may be dominated by the prompt emission. Only the long lasting emission in the time range from $T_0 + 3000$ s to $T_0 + 20000$ s can be well explained by the external-forward shock radiation from the jet only. The *Fermi*/LAT observations show

⁸ <https://ned.ipac.caltech.edu/forms/calculator.html>

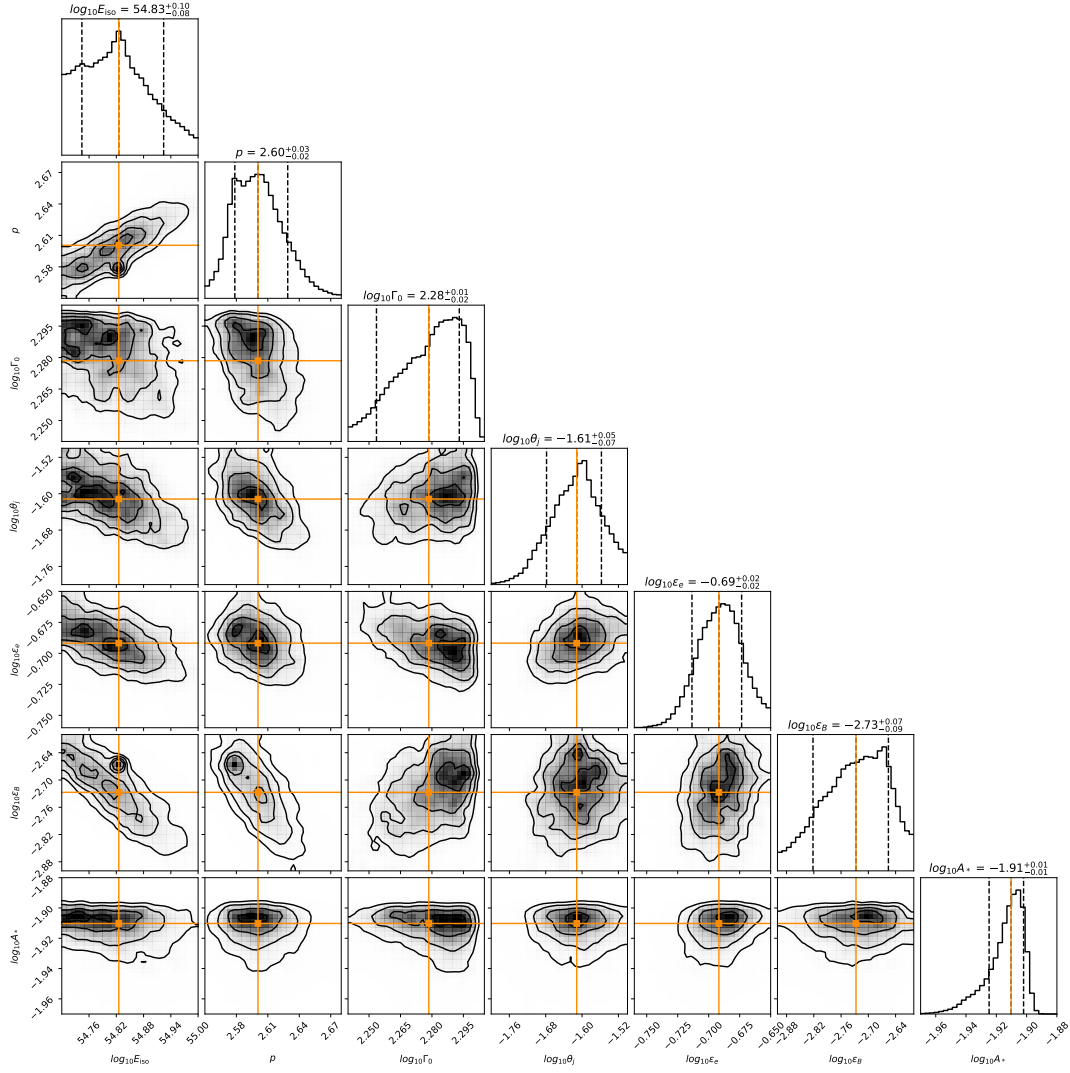


Figure 3. Contour plot for the posterior distributions of parameters.

GeV emission exceeding the model curve at later time $> T_0 + 20000$ s. This phenomenon is hardly explained by just external-forward shock origin. Notice that the precursor of GRB 221009A may be excited by the cocoon formed by the jet-envelope interaction. We suggest an explaining of this extra GeV emission by the EIC process of photons from cocoon cooling (e.g., He et al. 2009). Obviously, our model explains the X-ray, optical and radio band data quite well. The model light curves of radio bands lasting long and flat, consistent with the reported observations. It is worth noting that the excess of early ~ 15 GHz band radio observation to the model light curve is possibly due to the radiation from a reverse shock (de Ugarte Postigo et al. 2022a). We show the HAWC 95% upper limit on the flux at 1 TeV in Figure 2, and find our result satisfy this constraint.

Over all, we find no significant bumpy has shown in the late time observation lightcurves especially in the optical and X-ray band. So, the jet towards us of GRB 221009A seems propagate in a wind dominated environment with no significant density jump in the radial profile. Based on our inference result, the parameter describing the intensity of the wind $A_* = 1.2 \times 10^{-2}$, shows that the progenitor had a relatively small outflow of material prior to the burst. The micro physical parameters $\epsilon_e = 0.2$ and $\epsilon_B = 1.86 \times 10^{-3}$ lie within the typical value range. We notice that the half-opening angle of jet $\theta_j = 1^\circ.4$ is mainly determined by z band data we used, this value may be changed by observational data with better qualities. The combination of parameters is not exceptional, suggesting that GRB 221009A is a typical wind environment dominated long GRB. We calculated the efficiency of prompt emission to the total

energy of jet as $\eta_\gamma = E_{\gamma,\text{iso}}/(E_{\gamma,\text{iso}} + E_{k,\text{iso}}) \sim 23\% - 31\%$ which is consistent with the expectation of the fireball model (e.g., Lloyd-Ronning & Zhang 2004; Zhang et al. 2007). Furthermore, we find that the inclusion of GeV data partly breaks the parameter degeneracy commonly observed in GRB afterglow fitting (e.g., Ren et al. 2020), underlining the significance of high-energy data in determining accurate parameters for GRB afterglows. Based on the derived model parameters, we also calculated the maximum photon energy generated by the synchrotron radiation (Cheng & Wei 1996; Fan et al. 2013), which indicates that the high-energy photons come from inverse Compton radiation by comparing the *Fermi*/LAT observations (see Figure 4).

3.3. Spectral Energy Distribution

By using the parameters of fitting results, we show the SEDs of GRB 221009A afterglow in different timeslices, see Figure 5. We show the observed spectra data and corresponding fitting curves in Figure 5 within $T_0 + [4300, 5600]$ s for *Fermi*/LAT, and $T_0 + [3453, 4643]$ s for *Swift*/XRT, respectively. We also plot the SED of $T_0 + [220, 2000]$ s as a prediction result for the LHAASO observation spectrum. One can observe that the fit between the theoretical line and the observations is quite good in the X-ray and GeV bands. Comparing the sensitivity curves of LHAASO, MAGIC, and CTA, with the SED in our model, we find that the radiation in the 0.1–10 TeV band is extremely bright for detections during $T_0 + [220, 2000]$ s. Our model gives the maximum SSC radiation flux around 300 GeV, with the value of $\sim 10^{-7}$ erg cm $^{-2}$ s $^{-1}$. We find that the VHE radiation of GRB 221009A has been cut off around 10 TeV as a result of EBL absorption up to the redshift $z = 0.151$ (Domínguez et al. 2011). Compared with the sensitivity curve of LHAASO, the highest energy photons from the SSC process with energy of 11 TeV can be detected by LHAASO with 2000 seconds exposure by using the EBL model of Domínguez et al. (2011). If the 18 TeV photon detected by LHAASO at $T_0 + 2000$ s was realistic, it is hard to explain by the SSC mechanism only and suggest the existence of other radiation processes. Considering that EBL absorption has a rate of $e^{-\tau_{\text{EBL}}} \sim 10^{-8}$ at 18 TeV, the intrinsic flux required to account for the radiation process of this photon event is approximately larger than 10^{-2} erg cm $^{-2}$ s $^{-1}$ for the estimated sensitivity thresholds of LHAASO. This is corresponding to the radiation luminosity greater than $\sim 6.5 \times 10^{53}$ erg s $^{-1}$ at ~ 18 TeV. Some possibilities can explain this phenomenon, such as hadronic processes (e.g. synchrotron radiation of protons), Lorentz invariance violation (LIV)

and Axion-like particles (Li & Ma 2022), or the need for corrections to the EBL field of low-energy photons.

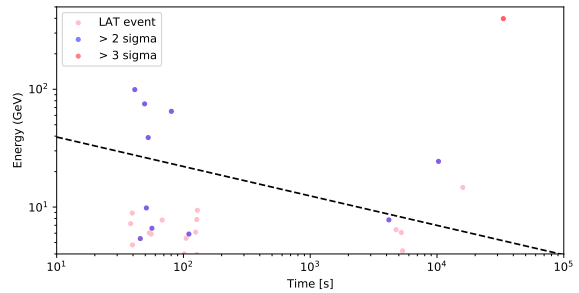


Figure 4. The red, blue, and pink dots represent photon events (> 5 GeV, within 1 degree) with different probabilities originating from GRB 221009A, respectively. The photon energy of the only red dot is 397.7 GeV, which is consistent with the result of Xia et al. (2022). The black dashed line is the maximum photon energy that synchrotron radiation can provide.

4. SUMMARY & DISCUSSION

In this paper, we have modeled the dynamics and radiation physics of the afterglow of the rarity event GRB 221009A in detail. The afterglow of GRB 221009A can be well explained by a relativistic jet with initial Lorentz factor $\Gamma_0 = 190$ propagating in an environment dominated by a stellar wind with parameter $A_\star = 1.2 \times 10^{-2}$. We have successfully explained the afterglow lightcurves and SEDs of GRB 221009A by using the synchrotron radiation plus the SSC mechanism. It makes GRB 221009A the first long GRB with clear indications of occurring in a wind environment to produce VHE afterglow. Our results show that the SSC component with photon energy large than 100 GeV is extremely bright during the first ~ 2000 seconds after the *Fermi*/GBM trigger time T_0 of GRB 221009A. The time integral SED within $T_0 + 220$ s to $T_0 + 2000$ s shows the SSC component has peaked in ~ 300 GeV and the peak flux $\nu F_\nu(300 \text{ GeV}) \sim 10^{-7}$ erg cm $^{-2}$ s $^{-1}$. Spectra above 300 GeV corrected with the EBL show an approximate power-law distribution up to 1 TeV, and rapidly drops with photon energies greater than 1 TeV before cut off at approximately 10 TeV. Our results indicate that the SSC component is very promising for the interpretation of VHE emission from GRB 221009A. If the 18 TeV event detected by LHAASO is realistic, we suggest an additional component (relative to the SSC component) to account for photons beyond 10 TeV, e.g., synchrotron radiation of protons. The corresponding luminosity of such a radiation process is required to have at least $\nu L_\nu \sim 6.5 \times 10^{53}$ erg s $^{-1}$ at 18 TeV. Also,

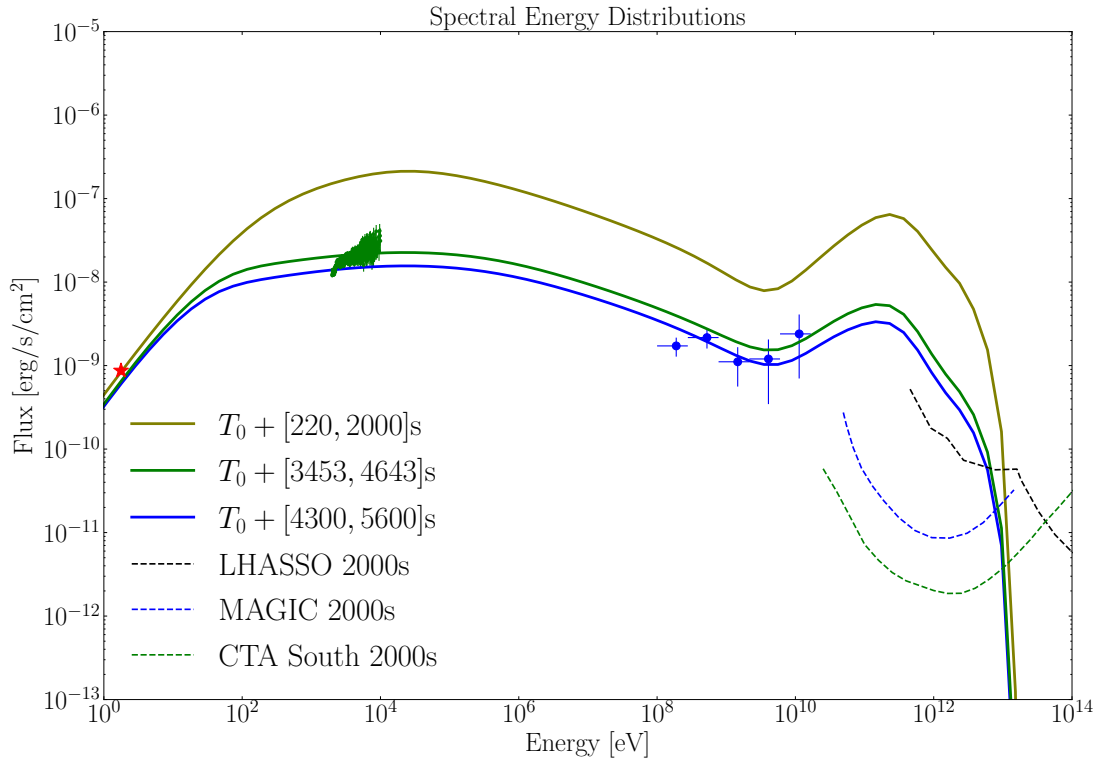


Figure 5. Afterglow SEDs of three chosen timeslices. The red star marks the R band data at $T_0 + 4150$ seconds from [Belkin et al. \(2022b\)](#), the green points mark the 2 – 10 keV *Swift*/XRT data within $T_0 + [3453, 4643]$ s, and the blue points mark the 0.1 – 10 GeV *Fermi*/LAT data within $T_0 + [4300, 5600]$ s, respectively. The black, blue, and green dashed lines correspond to the detection sensitivities of LHASO, MAGIC, and CTA in 2000 seconds, respectively ([Cao et al. 2019](#)).

other possible reasons such as Lorentz invariance violation (LIV) or corrections to the EBL field needs to be examined. Furthermore, we find that the inclusion of GeV data partly breaks the parameter degeneracy commonly observed in GRB afterglow fitting (e.g., [Ren et al. 2020](#)), underlining the significance of high-energy data in determining accurate parameters for GRB afterglows.

ACKNOWLEDGMENTS

This work was supported by the National Natural Science Foundation of China (grant No. 11833003). This work used data and software provided by the Fermi Science Support Center and data supplied by the UK Swift Science Data Centre at the University of Leicester. This research also used of the CTA instrument response functions provided by the CTA Consortium and Observatory, see <http://www.ctaobservatory.org/science/cta-performance/> (version prod3b-v2) for more details.

Software: `Matplotlib` ([Hunter 2007](#)), `Numpy` ([Harris et al. 2020](#)), `emcee` ([Foreman-Mackey et al. 2013](#)), `corner` ([Foreman-Mackey 2016](#)), `Astropy` ([Astropy Collaboration et al. 2013](#))

REFERENCES

- Abdalla, H., Adam, R., Aharonian, F., et al. 2019, *Nature*, 575, 464, doi: [10.1038/s41586-019-1743-9](https://doi.org/10.1038/s41586-019-1743-9)
- Acciari, V. A., Ansoldi, S., Antonelli, L. A., et al. 2021, *ApJ*, 908, 90, doi: [10.3847/1538-4357/abd249](https://doi.org/10.3847/1538-4357/abd249)
- Asano, K., Murase, K., & Toma, K. 2020, *ApJ*, 905, 105, doi: [10.3847/1538-4357/abc82c](https://doi.org/10.3847/1538-4357/abc82c)
- Astropy Collaboration, Robitaille, T. P., Tollerud, E. J., et al. 2013, *A&A*, 558, A33, doi: [10.1051/0004-6361/201322068](https://doi.org/10.1051/0004-6361/201322068)
- Atteia, J.-L. 2022, *GRB Coordinates Network*, 32793, 1
- Atwood, W., Abdo, A. A., Ackermann, M., et al. 2009, *The Astrophysical Journal*, 697, 1071
- Belkin, S., Nazarov, S., Pozanenko, A., & Pankov, N. 2022a, *GRB Coordinates Network*, 32684, 1
- Belkin, S., Pozanenko, A., E., K., & et al. 2022b, *GRB Coordinates Network*, 32645, 1
- Bikmaev, I., Khamitov, I., Irtuganov, E., et al. 2022a, *GRB Coordinates Network*, 32743, 1
- . 2022b, *GRB Coordinates Network*, 32752, 1
- Bissaldi, E., Omodei, N., Kerr, M., & et al. 2022a, *GRB Coordinates Network*, 32637, 1
- . 2022b, *GRB Coordinates Network*, 32637, 1
- Brethauer, D., Grefenstette, B., Racusin, J., et al. 2022, *The Astronomer's Telegram*, 15665, 1
- Bright, J., Rhodes, L., R., F., & et al. 2022, *GRB Coordinates Network*, 32653, 1
- Brivio, R., D'Avanzo, P., Fugazza, D., Melandri, A., & Covino, S. 2022, *GRB Coordinates Network*, 32652, 1
- Cao, Z., della Volpe, D., Liu, S., et al. 2019, *arXiv e-prints*, arXiv:1905.02773. <https://arxiv.org/abs/1905.02773>
- Castro-Tirado, A. J., Sanchez-Ramirez, R., Hu, Y.-D., & et al. 2022, *GRB Coordinates Network*, 32686, 1
- Chen, T.-W., Pan, Y.-C., Hsiao, H.-Y., Lin, C.-S., & Guo, J.-K. 2022, *GRB Coordinates Network*, 32667, 1
- Cheng, K., & Wei, D. 1996, *Monthly Notices of the Royal Astronomical Society*, 283, L133
- de Ugarte Postigo, A., Bremer, M., Thoene, C. C., & et al. 2022a, *GRB Coordinates Network*, 32676, 1
- de Ugarte Postigo, A., Izzo, L., Pugliese, G., & et al. 2022b, *GRB Coordinates Network*, 32648, 1
- de Wet, S., & Groot, P. 2022, *GRB Coordinates Network*, 32646, 1
- Dermer, C. D., Chiang, J., & Mitman, K. E. 2000, *ApJ*, 537, 785, doi: [10.1086/309061](https://doi.org/10.1086/309061)
- Dichiara, S., Gropp, J. D., Kennea, J. A., & Kuin, N. P. M. 2022, *GRB Coordinates Network*, 32632, 1
- Domínguez, A., Primack, J. R., Rosario, D. J., et al. 2011, *MNRAS*, 410, 2556, doi: [10.1111/j.1365-2966.2010.17631.x](https://doi.org/10.1111/j.1365-2966.2010.17631.x)
- Evans, P., Beardmore, A. P., Page, K. L., et al. 2007, *Astronomy & Astrophysics*, 469, 379
- Evans, P., Beardmore, A., Page, K., et al. 2009, *Monthly Notices of the Royal Astronomical Society*, 397, 1177
- Fan, Y. Z., & Piran, T. 2006, *MNRAS*, 369, 197, doi: [10.1111/j.1365-2966.2006.10280.x](https://doi.org/10.1111/j.1365-2966.2006.10280.x)
- Fan, Y. Z., Piran, T., Narayan, R., & Wei, D.-M. 2008, *MNRAS*, 384, 1483, doi: [10.1111/j.1365-2966.2007.12765.x](https://doi.org/10.1111/j.1365-2966.2007.12765.x)
- Fan, Y.-Z., Tam, P., Zhang, F.-W., et al. 2013, *The Astrophysical Journal*, 776, 95
- Farah, W., Bright, J., A., P., & et al. 2022, *GRB Coordinates Network*, 32655, 1
- Finke, J. D., Razzaque, S., & Dermer, C. D. 2010, *ApJ*, 712, 238, doi: [10.1088/0004-637X/712/1/238](https://doi.org/10.1088/0004-637X/712/1/238)
- Foreman-Mackey, D. 2016, *The Journal of Open Source Software*, 1, 24, doi: [10.21105/joss.00024](https://doi.org/10.21105/joss.00024)
- Foreman-Mackey, D., Hogg, D. W., Lang, D., & Goodman, J. 2013, *PASP*, 125, 306, doi: [10.1086/670067](https://doi.org/10.1086/670067)
- Fukami, S., Berti, A., Loporchio, S., et al. 2021, in *Proceedings of 37th International Cosmic Ray Conference — PoS(ICRC2021)*, Vol. 395, 788, doi: [10.22323/1.395.0788](https://doi.org/10.22323/1.395.0788)
- Geng, J.-J., Huang, Y.-F., Wu, X.-F., Zhang, B., & Zong, H.-S. 2018, *ApJS*, 234, 3, doi: [10.3847/1538-4365/aa9e84](https://doi.org/10.3847/1538-4365/aa9e84)
- Gould, R. J., & Schröder, G. P. 1967, *Physical Review*, 155, 1408, doi: [10.1103/PhysRev.155.1408](https://doi.org/10.1103/PhysRev.155.1408)
- Gregory, S. P., Myungshin, I., Yuji, U., & Hyun-I, S. 2022, *GRB Coordinates Network*, 32659, 1
- Groot, P., Vreeswijk, P., Ter Horst, R., et al. 2022, *GRB Coordinates Network*, 32678, 1
- H. E. S. S. Collaboration, Abdalla, H., Aharonian, F., et al. 2021, *Science*, 372, 1081, doi: [10.1126/science.abe8560](https://doi.org/10.1126/science.abe8560)
- Harris, C. R., Millman, K. J., van der Walt, S. J., et al. 2020, *Nature*, 585, 357, doi: [10.1038/s41586-020-2649-2](https://doi.org/10.1038/s41586-020-2649-2)
- HAWC collaboration. 2022, *GRB Coordinates Network*, 32683, 1
- He, H.-N., Wang, X.-Y., Yu, Y.-W., & Mészáros, P. 2009, *ApJ*, 706, 1152, doi: [10.1088/0004-637x/706/2/1152](https://doi.org/10.1088/0004-637x/706/2/1152)
- Hu, Y.-D., Casanova, V., Fernandez-Garcia, E., & Castro Tirado, M. A. 2022, *GRB Coordinates Network*, 32644, 1
- Huang, Y. 2022, *ApJ*, 931, 150, doi: [10.3847/1538-4357/ac6d52](https://doi.org/10.3847/1538-4357/ac6d52)
- Huang, Y., Hu, S.-C., Chen, S.-Z., & et al. 2022, *GRB Coordinates Network*, 32677, 1
- Huber, M., Schultz, A., Chambers, K., et al. 2022, *GRB Coordinates Network*, 32758, 1
- Hunter, J. D. 2007, *Computing in Science and Engineering*, 9, 90, doi: [10.1109/MCSE.2007.55](https://doi.org/10.1109/MCSE.2007.55)

- Hurley, K., Dingus, B. L., Mukherjee, R., et al. 1994, *Nature*, 372, 652, doi: [10.1038/372652a0](https://doi.org/10.1038/372652a0)
- Jiang, G.-S., & Shu, C.-W. 1996, *Journal of Computational Physics*, 126, 202, doi: [10.1006/jcph.1996.0130](https://doi.org/10.1006/jcph.1996.0130)
- Joshi, J. C., & Razzaque, S. 2021, *MNRAS*, 505, 1718, doi: [10.1093/mnras/stab1329](https://doi.org/10.1093/mnras/stab1329)
- Joshi, J. C., & Razzaque, S. 2021, *MNRAS*, 505, 1718, doi: [10.1093/mnras/stab1329](https://doi.org/10.1093/mnras/stab1329)
- Kim, V., Krugov, M., Pozanenko, A., et al. 2022, *GRB Coordinates Network*, 32670, 1
- Kuin, N., & Dichiara, S. 2022, *GRB Coordinates Network*, 32656, 1
- Kumar, H., Swain, V., Waratkar, G., et al. 2022, *GRB Coordinates Network*, 32662, 1
- Kumar, P., Hernández, R. A., Bošnjak, Ž., & Barniol Duran, R. 2012, *MNRAS*, 427, L40, doi: [10.1111/j.1745-3933.2012.01341.x](https://doi.org/10.1111/j.1745-3933.2012.01341.x)
- Laskar, T., Alexander, K. D., Ayache, E., & et al. 2022, *GRB Coordinates Network*, 32740, 1
- Li, H., & Ma, B.-Q. 2022, arXiv e-prints, arXiv:2210.06338. <https://arxiv.org/abs/2210.06338>
- Lloyd-Ronning, N. M., & Zhang, B. 2004, *ApJ*, 613, 477, doi: [10.1086/423026](https://doi.org/10.1086/423026)
- MAGIC Collaboration, Acciari, V. A., Ansoldi, S., et al. 2019, *Nature*, 575, 459, doi: [10.1038/s41586-019-1754-6](https://doi.org/10.1038/s41586-019-1754-6)
- Murase, K., Ioka, K., Nagataki, S., & Nakamura, T. 2006, *ApJL*, 651, L5, doi: [10.1086/509323](https://doi.org/10.1086/509323)
- Murase, K., Toma, K., Yamazaki, R., & Mészáros, P. 2011, *ApJ*, 732, 77, doi: [10.1088/0004-637x/732/2/77](https://doi.org/10.1088/0004-637x/732/2/77)
- Nakar, E., Ando, S., & Sari, R. 2009, *ApJ*, 703, 675, doi: [10.1088/0004-637X/703/1/675](https://doi.org/10.1088/0004-637X/703/1/675)
- Nava, L., Sironi, L., Ghisellini, G., Celotti, A., & Ghirlanda, G. 2013, *MNRAS*, 433, 2107, doi: [10.1093/mnras/stt872](https://doi.org/10.1093/mnras/stt872)
- Omodei, N., Bruel, P., Bregeon, J., et al. 2022, *GRB Coordinates Network*, 32760, 1
- Pe’er, A. 2012, *ApJL*, 752, 8, doi: [10.1088/2041-8205/752/1/L8](https://doi.org/10.1088/2041-8205/752/1/L8)
- Pei, Y. C. 1992, *ApJ*, 395, 130, doi: [10.1086/171637](https://doi.org/10.1086/171637)
- Pillera, R., Bissaldi, E., Omodei, N., La Mura, G., & Longo, F. 2022, *GRB Coordinates Network*, 32658, 1
- Planck Collaboration, Ade, P. A. R., Aghanim, N., et al. 2016, *A&A*, 594, A13, doi: [10.1051/0004-6361/201525830](https://doi.org/10.1051/0004-6361/201525830)
- Ren, J., Lin, D.-B., Zhang, L.-L., et al. 2020, *ApJ*, 901, L26, doi: [10.3847/2041-8213/abb672](https://doi.org/10.3847/2041-8213/abb672)
- Rhodes, L., Bright, J., Fender, R., & et al. 2022, *GRB Coordinates Network*, 32700, 1
- Sari, R., & Esin, A. A. 2001, *ApJ*, 548, 787, doi: [10.1086/319003](https://doi.org/10.1086/319003)
- Sari, R., & Piran, T. 1999, *ApJL*, 517, L109, doi: [10.1086/312039](https://doi.org/10.1086/312039)
- Sari, R., Piran, T., & Narayan, R. 1998, *ApJ*, 497, L17, doi: [10.1086/311269](https://doi.org/10.1086/311269)
- Schlegel, D. J., Finkbeiner, D. P., & Davis, M. 1998, *ApJ*, 500, 525, doi: [10.1086/305772](https://doi.org/10.1086/305772)
- Shrestha, M., Bostroem, K., Sand, D., Alexander, K. D., & et al. 2022a, *GRB Coordinates Network*, 32771, 1
- Shrestha, M., Sand, D., Alexander, K., et al. 2022b, *GRB Coordinates Network*, 32759, 1
- Strausbaugh, S., & Cucchiara, A. 2022, *GRB Coordinates Network*, 32693, 1
- Suda, Y., Artero, M., Asano, K., et al. 2021, in *Proceedings of 37th International Cosmic Ray Conference — PoS(ICRC2021)*, Vol. 395, 797, doi: [10.22323/1.395.0797](https://doi.org/10.22323/1.395.0797)
- Trushkin, S. A., Nizhelskij, N. N., Tsybulev, P. G., & Erkenov, A. K. 2022, *The Astronomer’s Telegram*, 15671, 1
- Urata, Y., Huang, K. Y., Covino, S., & et al. 2022, *GRB Coordinates Network*, 32761, 1
- Veres, P., Burns, E., Bissaldi, E., Lesage, S., & Roberts, o. 2022, *GRB Coordinates Network*, 32636, 1
- Vinko, J., Bodi, A., Pal, A., et al. 2022, *GRB Coordinates Network*, 32709, 1
- Wang, X.-Y., Liu, R.-Y., Zhang, H.-M., Xi, S.-Q., & Zhang, B. 2019, *ApJ*, 884, 117, doi: [10.3847/1538-4357/ab426c](https://doi.org/10.3847/1538-4357/ab426c)
- Watson, A., Butler, N., Dichiara, S., et al. 2022, *GRB Coordinates Network*, 32692, 1
- Waxman, E. 1997, *ApJL*, 485, L5, doi: [10.1086/310809](https://doi.org/10.1086/310809)
- Xia, Z.-Q., Wang, Y., Yuan, Q., & Fan, Y.-Z. 2022, *GRB Coordinates Network*, 32748, 1
- Xue, R., Tam, P., Wagner, S., et al. 2009, *The Astrophysical Journal*, 703, 60
- Yamasaki, S., & Piran, T. 2022, *MNRAS*, 512, 2142, doi: [10.1093/mnras/stac483](https://doi.org/10.1093/mnras/stac483)
- Zaznobin, I., Burenin, R., & Eselevich, M. 2022, *GRB Coordinates Network*, 32729, 1
- Zhang, B. 2018, *The Physics of Gamma-Ray Bursts*, doi: [10.1017/9781139226530](https://doi.org/10.1017/9781139226530)
- Zhang, B., & Mészáros, P. 2001, *ApJ*, 559, 110, doi: [10.1086/322400](https://doi.org/10.1086/322400)
- Zhang, B., Liang, E., Page, K. L., et al. 2007, *ApJ*, 655, 989, doi: [10.1086/510110](https://doi.org/10.1086/510110)
- Zhang, B. T., Murase, K., Yuan, C., Kimura, S. S., & Mészáros, P. 2021, *ApJL*, 908, L36, doi: [10.3847/2041-8213/abe0b0](https://doi.org/10.3847/2041-8213/abe0b0)
- Zhang, H., Christie, I. M., Petropoulou, M., Rueda-Becerril, J. M., & Giannios, D. 2020, *MNRAS*, 496, 974, doi: [10.1093/mnras/staa1583](https://doi.org/10.1093/mnras/staa1583)
- Zhang, L.-L., Ren, J., Huang, X.-L., et al. 2021, *ApJ*, 917, 95, doi: [10.3847/1538-4357/ac0c7f](https://doi.org/10.3847/1538-4357/ac0c7f)

Zheng, E., Zheng, W.-K., & Filippenko, A. V. 2022, GRB
Coordinates Network, 32669, 1